CHEMISTRY OF MATERIALS
Article

Chem. Mater. **2010,** *22,* 233–240 233
DOI:10.1021/cm9027995

ZnTe/ZnSe (Core/Shell) Type-II Quantum Dots: Their Optical and Photovoltaic Properties

Jiwon Bang,[†] Juwon Park,[†] Ji Hwang Lee,[‡] Nayoun Won,[†] Jutaek Nam,[†] Jongwoo Lim,[†] Byoung Yong Chang,[†] Hyo Joong Lee,[†] Bonghwan Chon,[†] Junghan Shin,[⊥] Jae Byung Park,[⊥] Jong Hwa Choi,[¶] Kilwon Cho,[‡] Su Moon Park,[§] Taiha Joo,[†] and Sungjee Kim*[,†]

[†]*Department of Chemistry, Pohang University of Science and Technology, San 31, Hyoja-Dong, Nam-Gu, Pohang, 790-784, South Korea,* [‡]*Department of Chemical Engineering, Pohang University of Science and Technology, San 31, Hyoja-Dong, Nam-Gu, Pohang, 790-784, South Korea,* [⊥]*Fundamental Technology Group1, LCD Division Device Solution Business, Samsung Electronics Co., Ltd, San 24, Nongseo-dong, Giheung-gu, Yongin, 446-711, South Korea,* [¶]*Neo Technology & Energy R&D Institute, Agency for Defense Development, Yuseong P.O. Box 35-4, Daejeon, 305-600, South Korea, and* [§]*School of Energy Engineering, Ulsan National Institute of Science & Technology, Banyeon-ri 100, Ulsan, 689-798, South Korea*

Received September 8, 2009. Revised Manuscript Received October 12, 2009

Synthesis of a size series of colloidal ZnTe/ZnSe (core/shell) quantum dots (QDs) is reported. Because of the unique Type-II characters, their emission can range over an extended wavelength regime, showing photoluminescence (PL) from blue to amber. The PL lifetime measures as long as 77 ns, which clearly indicates the Type-II characteristics. ZnTe/ZnSe (Core/Shell) QDs can be further passivated by ZnS layers, rendered in water, while preserving the optical and chemical stabilities and thus proved their potentials toward "nontoxic" biological or medical applications that are free from concerns regarding heavy-metal leakage. ZnTe/ZnSe Type-II QD/polymer hybrid organic solar cells are also showcased, promising environmentally friendly photovoltaic devices. ZnTe/ZnSe Type-II QD incorporated photovoltaic devices show 11 times higher power conversion efficiency, when compared to that of the control ZnSe QD devices. This results from the Type-II characteristic broad QD absorption up to extended wavelengths and the spatially separated Type-II excitons, which can enhance the carrier extractions. We believe that ZnTe/ZnSe-based Type-II band engineering can open many new possibilities as exploiting the safe material choice.

Introduction

Colloidal semiconductor quantum dots (QDs) are being extensively studied for many applications, including fluorescent cellular tagging,[1,2] whole-body imaging,[3−5] cancer therapy,[6] light-emitting diodes,[7−9] lasers,[10,11] and solar cells,[12−15] because of their novel optical and electrical properties from the three-dimensional confinement. Generally, QDs are desired to be nontoxic for biological or medical applications and to be environmentally friendly for display, lighting, and photovoltaic devices. It is of paramount importance to develop QDs that are free from the toxic concerns such as potential leakage of heavy-metal ions. Unfortunately, many semiconductors that can be exploited for QD applications contain toxic elements. For example, among the II−VI semiconductors, safe choices for QDs seem to be limited to ZnO, ZnS, ZnSe, or ZnTe. However, their large band gaps may severely limit their applicability, because they can hardly absorb or emit in visible ranges. Transition-metal-doped QDs (such as manganese-doped ZnSe QD) can, in part, circumvent the hurdle. However, their absorption is still mostly confined to the

*Author to whom correspondence should be addressed. Tel.: 82-54-279-2108. Fax: 82-54-279-1498. E-mail: sungjee@postech.ac.kr.

(1) Bruchez, M.; Moronne, M.; Gin, P.; Weiss, S.; Alivisatos, A. P. *Science* **1998**, *281*, 2013.
(2) Chan, W. C.; Nie, S. *Science* **1998**, *281*, 2016.
(3) Michalet, X.; Pinaud, F. F.; Bentolila, L. A.; Tsay, J. M.; Doose, S.; Li, J. J.; Sundaresan, G.; Wu, A. M.; Gambhir, S. S.; Weiss, S. *Science* **2005**, *307*, 538.
(4) Gao, X.; Cui, Y.; Levenson, R. M.; Chung, L. W. K.; Nie, S. *Nat. Biotechnol.* **2004**, *22*, 969.
(5) Cai, W.; Shin, D.-W.; Chen, K.; Gheysens, O.; Cao, Q.; Wang, S. X.; Gambhir, S. S.; Chen, X. *Nano Lett.* **2006**, *6*, 669.
(6) Shi, L.; Hernandez, B.; Selke, M. *J. Am. Chem. Soc.* **2006**, *128*, 6278.
(7) Coe, S.; Woo, W.-K.; Bawendi, M. G.; Bulovic, V. *Nature* **2002**, *420*, 800.
(8) Bowers, M. J.; McBride, J. R.; Rosenthal, S. J. *J. Am. Chem. Soc.* **2005**, *127*, 15378.
(9) Caruge, J. M.; Halpert, J. E.; Wood, V.; Buloví, V.; Bawendi, M. G. *Nat. Photonics* **2008**, *2*, 247.
(10) Klimov, V. I.; Mikhailovsky, A. A.; Xu, S.; Malko, A.; Hollingsworth, J. A.; Leatherdale, C. A.; Eisler, H.-J.; Bawendi, M. G. *Science* **2000**, *290*, 314.
(11) Klimov, V. I.; Ivanov, S. A.; Nanda, J.; Achermann, M.; Bezel, I. J.; McGuire, A.; Piryatinski, A. *Nature* **2007**, *447*, 441.
(12) Huynh, W. U.; Dittmer, J. J.; Alivisatos, A. P. *Science* **2002**, *295*, 2425.
(13) Gur, I.; Fromer, N. A.; Geier, M. L.; Alivisatos, A. P. *Science* **2005**, *310*, 462.
(14) Zhong, H.; Zhou, Y.; Yang, Y.; Yang, C.; Li, Y. *J. Phys. Chem. C* **2007**, *111*, 6538.
(15) Sun, B.; Marx, E.; Greenham, N. C. *Nano Lett.* **2003**, *3*, 961.

Published on Web 11/23/2009

ultraviolet (UV) region, and the emission wavelength is not flexibly tunable.[16−19]

Type-II band gap engineering can open a new window for the QD material choice. These core/shell heterostructured nanoparticles are composed of two semiconductor materials of which both of the valence and conduction bands in the cores are lower (or higher) in energy than those in the shells. As a result, one of the carriers is mostly confined in the core of the QD, while the other one remains in the shell. Their effective band gaps are heavily governed by the band offsets of the cores and shells.[20−22] Type-II QDs can have an effective band gap that is smaller than that of either the constituent core or shell. For example, CdTe/CdSe (core/shell, C/S) QDs can emit infrared radiation that is even beyond the bulk band gaps of either CdTe or CdSe, and thus can be successfully used for in vivo imaging.[23] Furthermore, the extended absorptions and spatial charge separations of Type-II QDs can be advantageous for photovoltaic applications.[14]

Herein, we report synthesis of colloidal Type-II ZnTe/ZnSe (C/S) QDs and their optical and photovoltaic properties. Recently, solution-liquid−solid synthesis of ZnSe/ZnTe (C/S) quantum wires has been reported by Buhro and co-workers.[24] Colloidal ZnTe/ZnSe (C/S) QDs have not been reported so far, and we address comprehensive studies on the optical and photovoltaic properties as well as the synthesis. Zinc, selenium, and tellurium are chosen to meet strict toxicity or environmental criteria, because they are commonly considered as micronutrients. Emissions from Type-II ZnTe/ZnSe (C/S) QDs range from blue to amber, demonstrating the Type-II character at extended wavelengths. ZnTe/ZnSe QD-conducting polymer solar cells are demonstrated and the photovoltaic properties are investigated. Additional protective ZnS shell layers can be also introduced for ZnTe/ZnSe/ZnS (core/shell/shell, or C/S/S) QDs to guarantee the chemical stability and enhanced photoluminescence (PL) quantum efficiency (QE). They can be rendered in aqueous media, making them promising for use in "nontoxic" biological or medical probe applications.

Experimental Section

Materials. Diethylzinc, selenium pellet (99.999+%, ~2 mm), tellurium shot (99.999%, 1−2 mm), tri *n*-octylphosphine (TOP, 90%), 1-hexadecylamine (HDA, 98%), 1-octadecene (ODE, 90%), anhydrous pyridine (99.8%), and anhydrous chlorobenzene (99.8%) were purchased from Aldrich. (±)-α-Lipoic acid was purchased from Sigma. Bis(trimethylsilyl)sulfide (95%) and tetramethylammonium hydroxide pentahydrate (99%) were purchased from Acros Organics. Regioregular electronics-grade poly(3-hexylthiophene-2,5-diyl) (P3HT) was purchased from Reike Specialty Polymers. Poly-3-4-ethylenedioxythiophene (PEDOT)/poly-4-sytrensulfonate (PSS) was purchased from Bayer (Baytron P AI 4083).

Synthesis of ZnTe QDs and ZnSe QDs. For ZnTe QD synthesis, 1 mmol of tellurium shots were dissolved by 2 mL of TOP in a glovebox, and that was mixed with 0.5 mmol of diethylzinc. ODE (2.3 mL) and 1.7 g HDA were loaded in a 50-mL 3-neck flask, dried under vacuum at 120 °C for 2 h, and heated to 270 °C under a nitrogen gas flow. At this temperature, the mixture of zinc and tellurium precursors was quickly injected into the reaction flask and stirred continuously until ZnTe QDs of desired size were obtained. The reaction mixture was cooled to room temperature and diluted by hexanes. To remove excess organics, the QD crude product was precipitated by excess methanol, collected by centrifugation, and redispersed by small amount of hexanes. ZnTe QDs were stored in darkness in a nitrogen gas environment.

ZnSe QDs were prepared using a method similar to that previously described. The selenium precursor was prepared by dissolving selenium pellets in TOP.

Synthesis of ZnTe/ZnSe (Core/Shell) Type-II QDs and ZnTe/ZnSe/ZnS (Core/Shell/Shell) QDs. For ZnSe shell deposition onto bare ZnTe QDs, 0.5 mmol diethylzinc and 0.5 mmol selenium pellets that were dissolved in 8 mL of TOP were mixed in a glovebox. ODE (8 mL) and 0.9 g HDA were loaded into a 50-mL four-neck flask. Under a nitrogen gas flow, bare ZnTe QDs were introduced into the reaction flask. When the temperature of the reaction flask reached 200 °C, the precursor mixture of zinc and selenium was added dropwise for 6 h, and the temperature was maintained at 200−250 °C. ZnTe/ZnSe (core/shell) QDs were purified using a method similar to that for bare ZnTe QDs. Outer ZnS shell deposition onto ZnTe/ZnSe (core/shell) QDs was performed immediately after the ZnSe shell deposition onto ZnTe QDs without purifications. The ZnTe/ZnSe (core/shell) QD product was cooled to 200 °C. A precursor mixture of 0.3 mmol diethylzinc and 0.3 mmol bis(trimethylsilyl)sulfide in 3.5 mL of TOP was added dropwise for 2 h, and stirred continuously for 1 h at 220 °C. The product ZnTe/ZnSe/ZnS (core/shell/shell) QDs were purified by precipitation with excess methanol.

Surface Modification of ZnTe/ZnSe/ZnS (Core/Shell/Shell) QDs. Dihydrolipoic acid (DHLA) was made using the following protocol.[25] (±)-α-Lipoic acid (2 mmol) and 4 mmol sodium borohydride were dispersed in 8 mL of deionized water and vigorously stirred for 20 min. Saturated HCl (~0.5 mL) was added into the reaction vessel. DHLA was obtained by extraction using chloroform. Surface ligand exchange of ZnTe/ZnSe/ZnS (core/shell/shell) QDs by DHLA was performed by a similar method previously reported.[26] Previously prepared DHLA and 46 nmol of ZnTe/ZnSe/ZnS (core/shell/shell) QDs were dissolved in ~2 mL of chloroform and stirred for 2 h at 40 °C. Upon completion of the surface ligand exchange, DHLA-capped QDs were precipitated by adding 50 mg of tetramethylammonium hydroxide pentahydrate and then were transferred to a water layer of pH 12. The pH was adjusted using 2 N NaOH

(16) Norris, D. J.; Yao, N.; Charnock, F. T.; Kennedy, T. A. *Nano Lett.* **2001**, *1*, 3.
(17) Pradhan, N.; Battaglia, D. M.; Liu, Y.; Peng, X. *Nano Lett.* **2007**, *7*, 312.
(18) Thakar, R.; Chen, Y.; Snee, P. T. *Nano Lett.* **2007**, *7*, 3429.
(19) Zhang, Y.; Gan, C.; Muhammad, J.; Battaglia, D.; Peng, X.; Xiao, M. *J. Phys. Chem. C* **2008**, *112*, 20200.
(20) Kim, S.; Fisher, B.; Eisler, H. J.; Bawendi, M. G. *J. Am. Chem. Soc.* **2003**, *125*, 11466.
(21) Chen, C. Y.; Cheng, C. T.; Lai, C. W.; Hu, Y. H.; Chou, P. T.; Chou, Y. H.; Chiu, H. T. *Small* **2005**, *1*, 1215.
(22) Dorfs, D.; Salant, A.; Popov, I.; Banin, U. *Small* **2008**, *4*, 1319.
(23) Kim, S.; Lim, Y. T.; Soltesz, E. G.; De Grand, A. M.; Lee, J.; Nakayama, A.; Parker, J. A.; Mihaljevic, T.; Laurence, R. G.; Dor, D. M.; Cohn, L. H.; Bawendi, M. G.; Frangioni, J. V. *Nat. Biotechnol.* **2004**, *22*, 93.
(24) Dong, A.; Wang, F.; Daulton, T. L.; Buhro, W. E. *Nano Lett.* **2007**, *7*, 1308.
(25) Gunsalus, I. C.; Barton, L. S.; Gruber, W. *J. Am. Chem. Soc.* **1956**, *78*, 1763.
(26) Clapp, A. R.; Goldman, E. R.; Mattoussi, H. *Nat. Protocols* **2006**, *1*, 1258.

aqueous solution. To remove free excess DHLAs, the QD aqueous solution was dialyzed twice using an Amicon 50 kDa MW cutoff centrifugal filtration kit.

Photovoltaic Device Fabrication. QDs in hexanes were precipitated by adding ethanol and collected by centrifugation. The collected QDs were dispersed in hexanes and precipitated again by ethanol. The purified QDs were collected by centrifugation and dried. For surface ligand exchange to pyridine, 100 mg of QDs were suspended in 15 mL pyridine and refluxed overnight under a nitrogen gas flow. Upon completion of the ligand exchange, QDs were purified twice by successive precipitation, centrifugation, and redispersion processes using hexanes as the antisolvent and pyridine as the dispersion solvent. Pyridine-capped QDs were dissolved in 1 mL of mixed solvent of chlorobenzene and pyridine (80/20, vol/vol) in a glovebox. For P3HT, a chlorobenzene solution was prepared by dissolving 20 mg of P3HT in 1 mL of chlorobenzene. The QD solution and P3HT solution were mixed in a glovebox. The weight percentages between the QD and P3HT were made to be 80:20. PEDOT:PSS was spincast at 5000 rpm onto glass substrates coated with 150 nm of indium tin oxide (ITO) (resistivity = 20 Ω/sq) and annealed at 120 °C for 20 min. The PEDOT:PSS-coated ITO glass substrate was transferred into a glovebox, and the QD/P3HT blended solution was spincast at 1500 rpm onto a PEDOT:PSS layer and annealed at 150 °C for 2 h. For P3HT-only device, P3HT chlorobenzene solution (20 mg of P3HT in 1 mL of chrolobenzene) was spincast at 2000 rpm onto PEDOT:PSS layer and annealed at 150 °C for 2 h. Finally, 6 Å of lithium fluoride and 150 nm of aluminum top electrodes were deposited by thermal evaporation sequentially. The active area of individual device was 0.052 cm^2.

Characterization. Transmission electron microscopy (TEM) images were taken with a JEOL Model JEM-1011 TEM microscope system. Absorption spectra were obtained on an Agilent Technology Model 8453 UV−vis spectrophotometer, and PL spectra were measured on a SPEX FluoroLog 3 (Jobin Yvon Horiba) spectrofluorometer. Time-resolved photoluminescence (TRPL) was measured using a time-correlated single photon counting (TCSPC) technique. The light source was a home-built cavity-dumped Ti:sapphire oscillator pumped by a frequency-doubled Nd:YVO_4 laser (Verdi, Coherent, Inc.). The center wavelength of the oscillator output at 760 nm was doubled to 380 nm to serve as an excitation light by the second harmonic generation (SHG) in a 200-μm lithium triborate (LBO) crystal. The repetition rate of excitation pulse was 380 kHz. TRPL was measured using the TCSPC system equipped with a micro channel plate photomultiplier tube (MCP-PMT) (Hamamatsu, Model R3809-51) that has been described elsewhere.[27] The instrument response function of the TCSPC system has a width of 42 ps, to provide 8 ps of time resolution with deconvolution. X-ray diffraction (XRD) measurements were performed using a Rigaku Model RINT 2100 diffractometer, which was equipped with a Cu Kα X-ray source, and samples for analysis were prepared on a glass substrate. The current−voltage ($I-V$) measurements of photovoltaic devices were performed under one-sun conditions, using a xenon lamp (1 kW, Oriel) and an AM 1.5 global filter, under a nitrogen atmosphere at room temperature. The illumination intensity was calibrated using a standard silicon photovoltaic with a protective KG5 filter precalibrated by the National Renewable Energy Laboratory. $I-V$ curves were measured with a Keithley Model 4200 source measurement unit. The photocurrents were recorded using a Keithley Model 236 source measurement unit under illumination with a 300-W xenon lamp and a single-grating monochromator (Dongwoo-optron). The impedance data were obtained by staircase cyclic voltammetry Fourier-transform electrochemical impedance spectroscopy (SCV-FTEIS). The SCV-FTEIS measurements were conducted using a homemade fast-rise potentiostat, which had a rise time of < 50 ns/V. Ascending staircase potential waves whose step height was 20 mV were generated by an Agilent Model 33120 Arbitrary Waveform Generator, with a scan rate of 100 mV/s for the staircase voltammetric experiment. A series of ascending or descending voltage steps applied and currents obtained thereof were acquired at a rate of 50 000 samples/s, using a National Instrument NI-5922 high-speed data acquisition system with 24-bit resolution. The data acquisition system was interfaced with a Pentium-4 personal computer (PC) through its PCI slot. After the data acquisition, both the potential and current data obtained from each potential step were segmented into a packet. Impedances were then computed by first transforming the derivative signals of the potential and current data into the frequency domain by a discrete Fourier transform method with frequencies ranging from 5 Hz to 26.9 kHz, followed by dividing the AC voltages by the AC currents obtained thereof. The upper frequency over 26.9 kHz was discarded because of the high-frequency noise encountered. The calculations were performed using a Matlab program, and circuit simulations were conducted to fit the observed data using the EG&G's ZSimpWin program. Details of the related theory of the SCV-FTEIS and its experimental validation have been published elsewhere.[28]

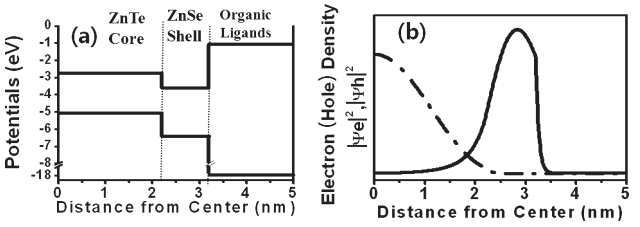

Figure 1. (a) ZnTe/ZnSe (2.2 nm radius core/1.0 nm thickness shell) QD is simulated for the potential diagram in radial direction and (b) the electron (solid line) and hole (dash-dotted line) residence probability densities. Bulk band alignments are used in reference to the vacuum level.[32]

Results and Discussion

ZnTe and ZnSe are direct-band-gap semiconductors with bulk band gaps of 540 and 443 nm, respectively. Both ZnTe and ZnSe have zincblende crystal structures, and they have a lattice mismatch of ~7% with each other. Colloidal ZnTe/ZnSe (C/S) Type-II QDs are synthesized by slightly modifying previously reported methods.[20−22,29−31] ZnTe cores are strictly kept in darkness and under inert gas conditions to prevent oxidation or decomposition. ZnSe shell deposition is typically performed at 220 °C. However, the deposition temperature is modified, depending on the core size and

(27) Chon, B.; Ryu, S. R.; Yoo, J.; Hong, Y.-J.; Yi, G.-C.; Joo, T.; Jung, Y. M. *J. Mol. Struct.* **2008**, *883−884*, 209.
(28) Chang, B. Y.; Hong, S. Y.; Yoo, J. S.; Park, S. M. *J. Phys. Chem. B* **2006**, *110*, 19386.
(29) Peng, X.; Schlamp, M. C.; Kadavanich, A. V.; Alivisatos, A. P. *J. Am. Chem. Soc.* **1997**, *119*, 7019.
(30) Hines, M. A.; Guyot-Sionnest, P. *J. Phys. Chem.* **1996**, *100*, 468.
(31) Dabbousi, B. O.; Rodriguez- Viejo, J.; Mikulec, F. V.; Heine, J. R.; Mattoussi, H.; Ober, R.; Jensen, K. F.; Bawendi, M. G. *J. Phys. Chem. B* **1997**, *101*, 9463.

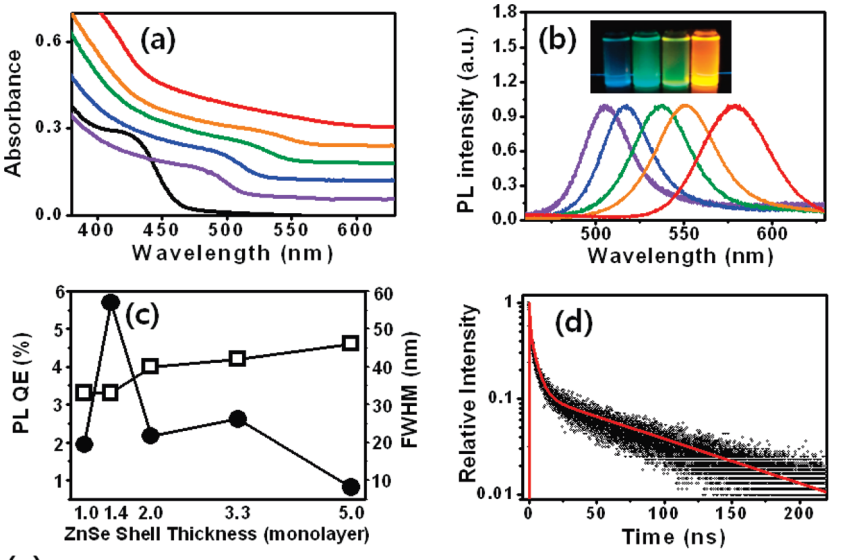

(e)

A_1 (%)	τ_1 (ns)	A_2(%)	τ_2 (ns)	A_3(%)	τ_3 (ns)	τ_{ave} (ns)	χ^2
51	0.59	39	4.8	10	94	77	1.21

Figure 2. (a) Absorption and (b) emission spectra of ZnTe/ZnSe (core/shell) QDs that have 2.2-nm-radius ZnTe cores and 1.0 (violet), 1.4 (blue), 2.0 (green), 3.3 (orange), and 5.0 (red) monolayers thick ZnSe shells. Black absorption spectrum represents 2.2 nm radius bare ZnTe QDs before the shell deposition. The inset in panel (b) shows various ZnTe/ZnSe (core/shell) QD samples under UV illumination. (c) Photoluminescence (PL) quantum efficiencies (closed circle, ●) and full widths at half-maximum (open squares, □) for ZnTe/ZnSe (core/shell) QDs with 2.2-nm-radius cores and different thicknesses of ZnSe shells. (d) Room-temperature normalized photoluminescence decay of ZnTe/ZnSe (2.2-nm-radius core/5-monolayer-thick shell) QD sample dispersed in hexanes. (e) Lifetime data extracted by a triexponent fit ($f(t) = \sum_{i=1}^{3} A_i e^{-(t/\tau_i)}$) from the PL decay; τ_{ave} is the intensity-weighted average lifetime, and χ^2 is the reduced chi-square value.

desired shell thickness. Higher temperatures are used to overcoat larger ZnTe cores, which is also typical for other QD overcoatings.[31]

Figure 1a shows simulated radial potential diagram for a ZnTe/ZnSe (C/S) QD. The bulk conduction and valence-band energy levels are used with reference to the vacuum level.[32] ZnTe and ZnSe show Type-II band alignment, where both conduction and valence bands of ZnTe lie at energies higher than those of ZnSe. As simulated in Figure 1b, an electron−hole pair in ZnTe/ZnSe (C/S) QD is supposed to show spatially separated distributions in which the hole mostly resides in the core, whereas the electron remains in the shell, because of the Type-II band offset. The effective band gap is heavily governed by the band offset between the valence level of ZnTe and the conduction level of ZnSe. ZnTe QDs on ZnSe buffer layers grown via the Stranski−Krastanov vapor deposition method have been reported to show Type-II characteristics, such as the emissions at extended wavelengths.[33,34]

Figures 2a and 2b show the continuous red shift in absorption and emission as depositing ZnSe shells onto ZnTe cores. A spectra shift as large as ∼100 nm is observed as up to 5 monolayers of ZnSe shells are deposited onto 2.2-nm radius ZnTe cores. This clearly indicates the strong Type-II characteristics as the excitons become more spatially separated by thicker shells. Initial bare ZnTe QDs show the distinctive band-edge absorption peak at ∼430 nm. As the ZnSe shell deposition proceeds, the absorption reaches to the longer wavelengths down to ∼600 nm and becomes more featureless. The bare ZnTe QDs are not emissive, presumably due to the unstable surfaces that are prone to nonradiative traps. The trap sites are thought to be passivated by ZnSe shell deposition, and the ZnTe/ZnSe (C/S) QDs become emissive. The PL of ZnTe/ZnSe (C/S) QDs ranges from 500 to 580 nm, covering from blue to amber color, as shown in the inset of Figure 2b. Figure 2c shows the changes in PL QE and PL full width at half-maximum (fwhm) for a series of ZnTe/ZnSe (C/S) QDs of different shell thicknesses. For thin ZnSe shell ZnTe/ZnSe (C/S) QDs, the passivation effect dominates and the PL QE improves as the shell thickness increases. The brightest sample among the shell thickness series shows the PL QE to be ∼6% with the 1.4-monolayer-thick ZnSe shell. However, thicker ZnSe shells begin to decrease the PL, because of the enhanced Type-II spatial separations between electrons and holes.[20−22] As shown in Figure 2c, PL bandwidth increases gradually as thicker ZnSe shells deposit onto ZnTe cores. The bandwidth is mostly governed by the inhomogeneous broadening from the size distribution of the sample. In the case of Type-II QDs, the size inhomogeneity can be considered as a convolution of the core size and the shell thickness distributions. As a result, the PL bandwidth should be more sensitive to the shell thickness when compared to conventional Type-I core−shell QDs.

(32) Pearton, S. J. *Wide Bandgap Semiconductors*; William Andrew Publishing: New York, 2000; p 9.
(33) Kuskovsky, I. L.; Tian, C.; Neumark, G. F.; Spanier, J. E.; Herman, I. P.; Lin, W.-C.; Guo, S. P.; Tamargo, M. C. *Phys. Rev. B* **2001**, *63*, 155205.
(34) Lee, J.; Yang, C. S.; Chang, C. T.; Liu, J.; Chou, W. C.; Lai, C. M.; Jan, G. J.; Huang, Y. S. *Phys. Status Solidi B* **2004**, *241*, 3532.

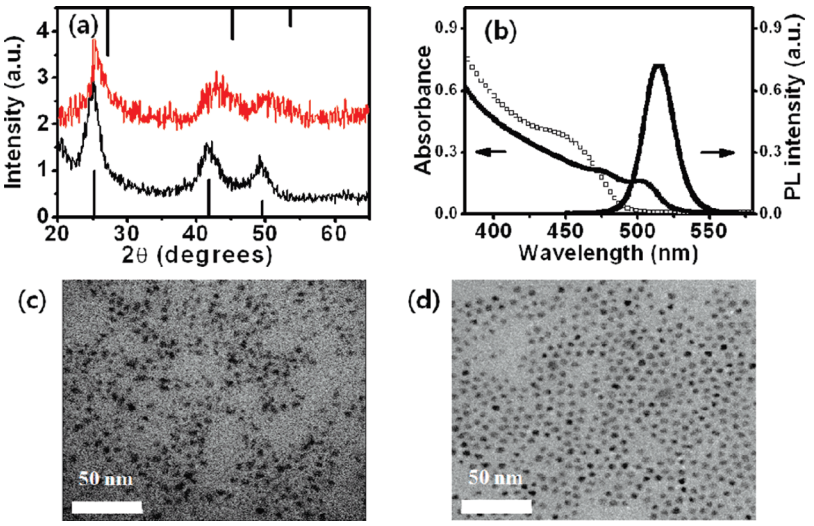

Figure 3. (a) Powder XRD patterns of 2-nm-radius ZnTe QDs (black line) and ZnTe/ZnSe (2-nm-radius core/1.3-nm-thick shell) QDs (red line). Bars on top and bottom represent bulk cubic structures of ZnSe and ZnTe, respectively. (b) Absorption spectrum of bare ZnTe QDs (open squares, □) and absorption and emission spectra of ZnTe/ZnSe (core/shell) QDs (closed squares, ■). TEM images of the (c) ZnTe QDs and (d) ZnTe/ZnSe (core/shell) QDs are shown, the optical properties of which are shown in panel (b).

For example, the ZnS shell thickness should have a lesser effect for the PL bandwidth, in the case of CdSe/ZnS (C/S) QDs.[31] Our ZnTe/ZnSe (C/S) QDs show the PL bandwidth of 30−50 nm, which is comparable to conventional Type-I QDs. This demonstrates the size uniformity of our QD preparation. Figure 2d shows PL decay of a ZnTe/ZnSe (C/S) QD sample dispersed in hexanes. The ZnTe/ZnSe (C/S) QD sample with the thickest shell (5 ML) was selected for the PL decay measurement to contrast the prominent Type-II characteristics. Because the absorption and emission spectra of the sample can be found by the red lines in Figures 2a and 2b, the absorption tail in the sample extends to ~570 nm and the emission peak is located at 580 nm. The PL decay measurement was performed at the emission peak using an excitation wavelength of 380 nm. The intensity-weighted average lifetime[35] and parameters extracted by a triexponential fitting are shown in the table that is presented in Figure 2e. The intensity-weighted average lifetime is measured to be 77 ns, which is significantly longer than Type-I QDs of similar size.[36,37] This undoubtedly reveals the Type-II characteristics of our ZnTe/ZnSe QDs as demonstrating the spatially separated excitons.[20−22] This rules out the possibility of alloyed ZnSeTe QD structures. In addition, the ZnTe/ZnSe (C/S) QDs show the PL wavelength at ~580 nm, which cannot be reached by an alloyed structure. Simple band-gap calculation shows that the minimum band gap (i.e., the most band bowed) composition of ZnSeTe alloyed QD should have a band gap of 540 nm when the same size as the 580-nm emitting ZnTe/ZnSe (C/S) QD is used for simulation, considering the quantum confinement effect.[38,39] Unfortunately, comparison between the bare ZnTe QDs could not be made, because they showed no detectable PL. The PL decay curve of the ZnTe/ZnSe (C/S) QD sample consists of the two fast components and one slow component. The QD sample has relatively low PL QE (~1%), because thicker ZnSe shells are presumably more prone to interface and/or surface-oriented defect sites, because of the large pressures applied by the crystal lattice mismatch. Extended exciton lifetime by the strong Type-II character may also increase the probability of nonradiative decay channels, by allowing the carriers to be trapped in the defect sites. We speculate that the first two fast components are more dominated by the nonradiative channels, whereas the slow component reveals the Type-II characteristic radiative decay. Similar instantaneous fast decay components have been also reported for CdTe/CdSe (C/S) QD samples.[40] However, CdTe/CdSe (C/S) QD PL decays reported by Bawendi and co-workers do not show the fast components.[20] The discrepancy is thought to originate from the QD quality and sample preparation difference. Because ZnTe/ZnSe (C/S) QDs are more sensitive to light and environment when compared to CdTe/CdSe (C/S) QDs, they may be more vulnerable to defect sites, which result in the instantaneous fast decays. The slow decay component measures as 94 ns, showing the characteristic long lifetime of Type-II QD, as this component is more contributed by the radiative decay channel.

Figure 3 shows powder X-ray diffraction (XRD) (Figure 3a), absorption and emission spectra (Figure 3b), and TEM images (Figures 3c and 3d) of an initial bare ZnTe QD sample and the overcoated ZnTe/ZnSe (C/S) QD sample. The crystal structure in both samples is elucidated by XRD to be zincblende. Bars on the top and bottom represent bulk cubic structures of ZnSe and ZnTe, respectively. XRD peaks become broadened and shifted to

(35) James, D. R.; Liu, Y. S.; Demayo, P.; Ware, W. R. *Chem. Phys. Lett.* **1985**, *120*, 460.
(36) Huang, H.; Dorn, A.; Nair, G. P.; Bulovic, V.; Bawendi, M. G. *Nano Lett.* **2007**, *7*, 3781.
(37) Lim, S. J.; Chon, B.; Joo, T.; Shin, S. K. *J. Phys. Chem. C* **2008**, *112*, 1744.
(38) Ebina, A.; Yamamoto, M.; Takahashi, T. *Phys. Rev. B* **1972**, *6*, 3786.
(39) Brus, L. E. *J. Chem. Phys.* **1983**, *79*, 5566.
(40) Oron, D.; Kazes, M.; Banin, U. *Phys. Rev. B* **2007**, *75*, 035330.

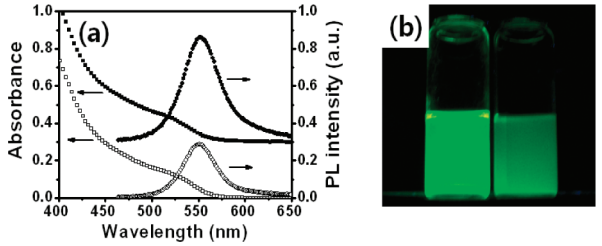

Figure 4. (a) Absorption and emission spectra of a ZnTe/ZnSe (core/shell) QD sample (open circles, ○) and a ZnTe/ZnSe/ZnS (core/shell/shell) QD sample (closed circles, ●). Both samples share identical ZnTe/ZnSe (core/shell) structures, because the outermost ZnS shells of the ZnTe/ZnSe/ZnS (core/shell/shell) QDs are deposited onto the ZnTe/ZnSe (core/shell) QDs. (b) Green-emitting ZnTe/ZnSe/ZnS (core/shell/shell) QDs are dispersed in hexanes (left) and in water (right) under UV illumination.

larger angles as ZnSe shells deposited onto ZnTe cores. Absorption spectrum red-shifts upon the overcoating, and the overcoated ZnTe/ZnSe (C/S) QD sample shows the emission wavelength that is even beyond the bulk ZnTe band gap. The size distribution becomes narrower after the overcoating as the size distribution decreases from 14% to 9.6%. This suggests that our overcoating condition is in the size-focusing regime and that the shell deposition proceeds rapidly, presumably because of the unstable ZnTe surfaces.[41,42]

ZnTe/ZnSe (C/S) QDs can be further passivated by introducing outermost ZnS shells for enhanced chemical stability. Based on the band offset, ZnS can confine both electrons and holes and thus should add small perturbation to the exciton characteristics. Figure 4a shows the absorption and emission spectra for a ZnTe/ZnSe (C/S) QD sample and the second shell layer overcoated ZnTe/ZnSe/ZnS (C/S/S) QD sample. Slight red shifts (~2 nm) are observed for both absorption and emission, which is typical for Type-I core/shell overcoating.[29−31] Because the outer ZnS shells effectively protect the inner ZnTe/ZnSe (C/S) structures, the PL intensity can be improved by more than 2-fold. Besides, ZnTe/ZnSe/ZnS (C/S/S) QDs can endure conventional surface ligand exchanges without the severe cost of PL intensity diminishment or colloidal stability deterioration. The double-shell QDs can be rendered water-soluble, for example, through ligand-exchange with dihydrolipoic acid. Figure 4b shows strong emissions from ZnTe/ZnSe/ZnS (C/S/S) QDs dispersed in an organic solvent and in water. Water-soluble ZnTe/ZnSe/ZnS (C/S/S) QDs can promise "nontoxic" fluorescent probes for biological and medical applications, because they do not possess potential toxicity concerns of heavy-metal-ion leakages (see the Supporting Information).

ZnTe/ZnSe (C/S) QDs can be advantageous for photovoltaic applications, not only because of the environmentally friendliness but also because of the broad absorption and spatially separated Type-II excitons that may enhance the carrier separation and extraction.[14,20−22] QD/polymer hybrid solar cells were assembled with ZnTe/ZnSe (C/S) QDs and poly(3-hexylthiophene) (P3HT), using previously reported methods.[12] ZnSe QDs were used in place of ZnTe/ZnSe (C/S) QDs for control devices. ZnSe QD, not ZnTe QD, was chosen for the control to match the final Fermi level with ZnTe/ZnSe (C/S) QD. A P3HT-only device also was fabricated for another control device. Figure 5a shows the potential diagram that illustrates the charge transfer between ZnTe/ZnSe (C/S) QD and P3HT. Electrons in P3HT can transfer to the ZnSe shells in ZnTe/ZnSe (C/S) QDs. Holes generated in ZnTe/ZnSe (C/S) QDs are supposed to be more localized in the cores. They must tunnel through the thin ZnSe shell barriers to reach the HOMO levels of P3HT. Figure 5b shows the extended absorption spectrum of ZnTe/ZnSe (C/S) QDs, when compared to that of ZnSe QDs. ZnSe QDs cannot efficiently absorb visible light, and, thus, their role is limited to the electron acceptor from photoexcited P3HT. In contrast, in addition to the role as an electron acceptor, ZnTe/ZnSe (C/S) QDs may be able to absorb visible wavelengths, generate spatially separated excitons, and transfer the holes to P3HT.

$I-V$ characteristics are investigated for the ZnTe/ZnSe (C/S) QD/P3HT device and the control ZnSe QD/P3HT device (see Figure 5c). The ZnTe/ZnSe (C/S) QD/P3HT device shows increased short circuit current density (J_{sc}) and open circuit voltage (V_{oc}) over the ZnSe QD control device. The ZnTe/ZnSe (C/S) QD/P3HT hybrid solar cell shows 11 times greater overall power conversion efficiency than that of the ZnSe QD control device. The efficiency is also 2 times higher than that of the P3HT-only photovoltaic device. Characteristic photovoltaic properties of the devices are listed in Table 1. Figure 5d compares external quantum efficiency (EQE) measurements of the ZnTe/ZnSe QD device and the ZnSe QD control device. ZnTe/ZnSe QDs exploit broader solar spectrum than ZnSe QDs and thus create photoexcited charge carriers to the extended wavelengths. Note that the EQE profile of the ZnTe/ZnSe QD device resembles the absorption spectrum. This indicates that the broader absorption by ZnTe/ZnSe QDs contributes to the enhanced power conversion efficiency. The efficiency enhancement may also originate from the loosely bound carriers that are generated by Type-II excitons. For both devices, impedance measurements are performed at 0 V under one-sun conditions to study the resistivity and capacity changes by different QD devices (see Figure 5e). Enhanced conductivity is observed for the ZnTe/ZnSe QD device, which corroborates more-efficient charge separations and transfers of the Type-II QD device. However, our ZnTe/ZnSe QD-based solar cells do not show high energy conversion efficiencies. We believe that the concentric core−shell ZnTe/ZnSe structure has limited us from fully exploiting the Type-II heterostructures for the photovoltaic application and, thus, obtaining high power conversion efficiency. It has been reported that aniso tropic semiconductor nanostructures such as nanorods[12] or tetrapods[15] can be more advantageous for photovoltaic

(41) Peng, X.; Wickham, J.; Alivisatos, A. P. *J. Am. Chem. Soc.* **1998**, *120*, 5343.
(42) Talapin, D. V.; Rogach, A. L.; Kornowski, A.; Haase, M.; Weller, H. *Nano Lett.* **2001**, *1*, 207.

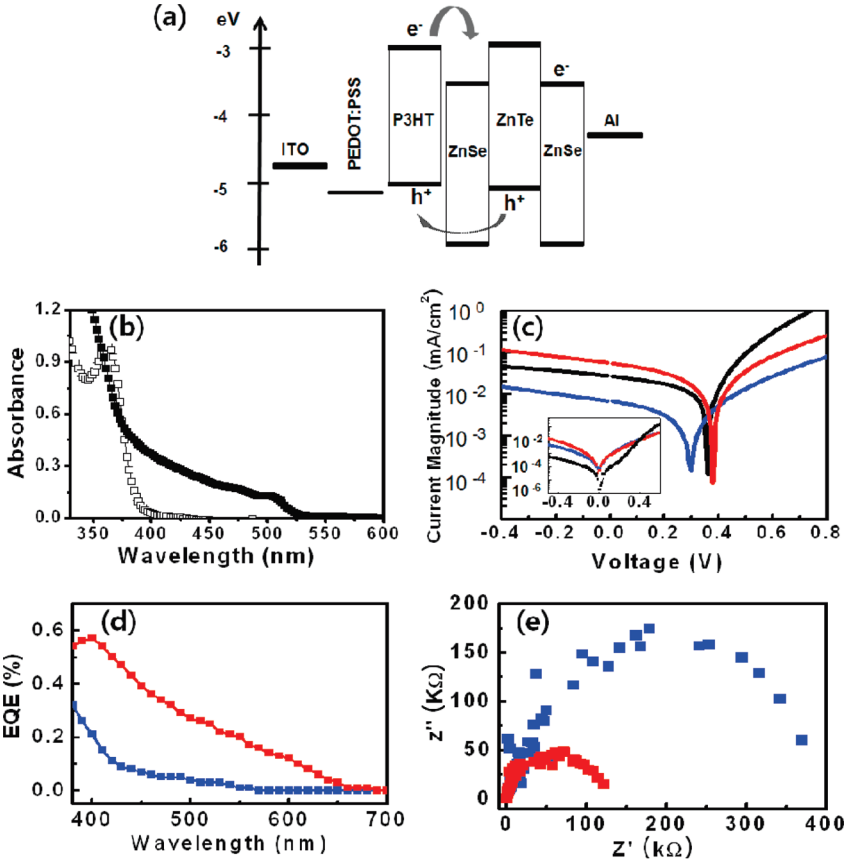

Figure 5. (a) Potential diagram for the photovoltaic device components referenced to the vacuum level. Bulk ZnTe and ZnSe energy levels are used.[32] (b) Absorption spectrum of (open squares, □) ZnSe QDs and (closed squares, ■) ZnTe/ZnSe (core/shell) QDs. (c) Semilogarithmic plot of $I-V$ curves for the ZnTe/ZnSe (core/shell) QD/P3HT device (red), the ZnSe QD/P3HT device (blue), and the P3HT-only device (black) measured under one-sun Air Mass 1.5 Global solar conditions. Inset shows a semilogarithmic plot of $I-V$ curves measured in darkness. (d) External quantum efficiency for the ZnTe/ZnSe (core/shell) QD/P3HT device (red) and ZnSe QD/P3HT device (blue). (e) Impedance plots of the ZnTe/ZnSe (Core/Shell) QD/P3HT photovoltaic device (red) and the ZnSe QD/P3HT contorl device (blue) measured at 0 V under one-sun Air Mass 1.5 Global solar conditions.

Table 1. Characteristic Photovoltaic Properties of the ZnTe/ZnSe (Core/Shell) QD/P3HT Photovoltaic Device, the ZnSe QD/P3HT Control Device, and the P3HT-Only Device

sample	short circuit current density, J_{sc} (mA/cm^2)	open circuit voltage, V_{oc} (V)	fill factor, FF	power conversion efficiency, PCE (%)
ZnTe/ZnSe QD/P3HT	0.055	0.38	0.30	6.3×10^{-3}
ZnSe QD/P3HT	0.0067	0.27	0.31	5.6×10^{-4}
P3HT	0.027	0.36	0.37	3.6×10^{-3}

applications. The anisotropic shape effect is expected to be much larger for Type-II cases. For example, ZnTe/ZnSe nanorods (with ZnTe on one end and ZnSe on the other end) or ZnTe/ZnSe tetrapods should have more-efficient hole extractions than our devices, because they do not have the ZnSe barriers. Recently, the syntheses of anisotropic Type-II nanostructures are being rapidly developed, such as CdTe/CdSe nanorods,[43] nanobarbells,[44] or branched tetrapods.[45] We expect that ZnTe/ZnSe Type-II based anisotropic nanostructures can promise environmentally friendly and efficient photovoltaic applications.

Conclusions

We have synthesized a size series of colloidal ZnTe/ZnSe (core/shell) quantum dots (QDs) with photoluminiscence (PL) quantum efficiency (QE) of up to 6%. Their emission can be tuned, ranging over a large portion of visible wavelengths, from blue to amber, because of the Type-II characters. Their Type-II characteristics were further elucidated by PL decay measurements, which exhibit a long average lifetime of 77 ns. They can be further passivated by ZnS layers, and they can be rendered in water while preserving the optical and chemical stabilities. They prove the potential toward "nontoxic" biological or medical applications that are free from heavy-metal-leakage concerns. ZnTe/ZnSe Type-II QD/polymer hybrid organic solar cells are showcased, promising environmentally friendly and efficient photovoltaic devices. We believe that ZnTe/ZnSe-based Type-II band engineering can open many new possibilities to exploiting the safe material choice.

Acknowledgment. This study was supported by a grant from the Korea Health 21 R&D Project, Ministry of

(43) Shieh, F.; Saunders, A. E.; Korgel, B. A. *J. Phys. Chem. B* **2005**, *109*, 8538.
(44) Halpert, J. E.; Porter, V. J.; Zimmer, J. P.; Bawendi, M. G. *J. Am. Chem. Soc.* **2006**, *128*, 12590.
(45) Milliron, D. J.; Hughes, S. M.; Cui, Y.; Manna, L.; Li, J.; Wang, L.-W.; Alivisatos, A. P. *Nature* **2004**, *430*, 190.

Health & Welfare, Republic of Korea (A060660), a Korea Science and Engineering Foundation (KOSEF) grant funded by the Korean government (MOST) (R0A-2008-000-20114-0-(2008), M10703001036-08M0300-03610, M10755020003-07N5502-00310), a Korea Research Foundation Grant (KRF-2008-331-C00140, KRF-2008-005-J00501), and the Defense Acquisition Program Administration and Agency for Defense Development (under Contract No. ADD-08-11-03).

Supporting Information Available: Concentration-dependent cell viability assay results on Cd and Zn ions. This material is available free of charge via the Internet at http://pubs.acs.org.